Journal of Geophysical Research: Space Physics

RESEARCH ARTICLE
10.1029/2018JA025679

Key Points:
- We study the dayside dynamics associated with the interaction of an interplanetary directional tangential discontinuity (TD) with the Earth's bow shock and magnetosphere
- The occurrence and structure of the magnetosheath reconnection depending on the structure of the TD and the geometry of the bow shock
- Magnetic reconnection may be initiated in the global magnetosheath prior to the magnetopause reconnection before the transmitted TD with a southward turning IMF reaches the magnetopause

Supporting Information:
- Supporting Information S1
- Movie S1

Correspondence to:
Y. Lin,
linyu01@auburn.edu

Citation:
Guo, Z., Lin, Y., Wang, X., & Du, A. (2018). Magnetosheath reconnection before magnetopause reconnection driven by interplanetary tangential discontinuity: A three-dimensional global hybrid simulation with oblique interplanetary magnetic field. *Journal of Geophysical Research: Space Physics*, *123*, 9169–9186. https://doi.org/10.1029/2018JA025679

Received 16 MAY 2018
Accepted 24 SEP 2018
Accepted article online 31 OCT 2018
Published online 12 NOV 2018

Magnetosheath Reconnection Before Magnetopause Reconnection Driven by Interplanetary Tangential Discontinuity: A Three-Dimensional Global Hybrid Simulation With Oblique Interplanetary Magnetic Field

Zhifang Guo[1,2], Yu Lin[3], Xueyi Wang[3], and Aimin Du[1,2]

[1]Key Laboratory of Earth and Planetary Physics, Institute of Geology and Geophysics, Chinese Academy of Sciences, Beijing, China, [2]Institutions of Earth Sciences, University of Chinese Academy of Sciences, Beijing, China, [3]Physics Department, Auburn University, Auburn, AL, USA

Abstract Terrestrial dayside dynamics associated with a southward turning, oblique interplanetary magnetic field (IMF) carried by an interplanetary tangential discontinuity (TD) is investigated by performing a three-dimensional global-scale hybrid simulation systematically for cases in which the incoming solar wind TD possesses various magnetic field rotation angles $\Delta\Phi = 90°$ to 180° and half widths $w = 2d_{i0}$ to $w = 30d_{i0}$, where d_{i0} is the ion inertial length in the solar wind. Overall, the TD is compressed while being transmitted into the magnetosheath, with different compression processes downstream of the quasi-parallel (Q-||) and quasi-perpendicular (Q-⊥) shocks. It is found that magnetosheath reconnection may take place downstream of both the Q-|| and Q-⊥ shocks due to interaction of the directional TD with the bow shock and magnetopause, but the existence of magnetosheath reconnection depends on w and $\Delta\Phi$. Magnetosheath flux ropes are formed through three-dimensional patchy reconnection in the thinned current sheet, with a longer rope lengths under a larger $\Delta\Phi$. There exists a dawn-dusk asymmetry in the spatial extent of the flux ropes, which becomes more significant as $\Delta\Phi$ decreases. When $\Delta\Phi$ decreases to 90°, no reconnection flux ropes are found. Magnetopause reconnection is initiated when the magnetic fluxes with a southward turning IMF (on the sunward side) reach the magnetopause, and the magnetopause flux ropes can be mixed with the magnetosheath ones. Our simulation demonstrates that the effects of a southward turning of the IMF may not be a simple field direction change that leads to reconnection only at the magnetopause.

1. Introduction

Four types of MHD discontinuities are determined by MHD Rankine-Hugoniot jump conditions: MHD shocks, contact discontinuity, tangential discontinuity (TD), and rotational discontinuity (RD). RDs and TDs have frequently been observed in the solar wind (e.g., Behannon et al., 1981; Burlaga et al., 1977; Lepping & Behannon, 1986; Tsurutani & Smith, 1979). RDs can be considered as Alfven waves, with a large-amplitude transverse magnetic field perturbation and a nonzero normal field component. TDs can be treated as a current sheet or static magnetic boundary layer without a mass flow and magnetic field component normal to the discontinuity. Across a TD, the total pressure is conserved, and the discontinuity simply convects with the plasma flow. Both interplanetary TDs and RDs are found to be closely associated with the trigger of the substorm expansion onset (Lyons et al., 1997), the sudden changes of the ionospheric convection pattern (Maynard et al., 2002), and the formation of a geomagnetic storm (Thomsen et al., 2003).

MHD discontinuities that possess only the magnetic field direction change but no plasma variations are often classified as directional discontinuities (DDs). They are primarily RDs or TDs. The DDs are frequently present in the solar wind, and they are of great interest in space physics (Burlaga, 1969, 1971; Burlaga et al., 1977; Lepping & Behannon, 1986) because of their strong nonlinear impacts to the magnetosphere in spite of little plasma density and pressure change in the incoming discontinuity. The simulation of Lin et al. (1996) has shown that the interaction of an RD with the bow shock and magnetosphere may not be a simple turning of the magnetic field direction, and it may produce dynamic pressure pulses impinging on the magnetopause, leading to magnetic impulse events. Primarily, two types of the interaction between an interplanetary TD and the bow shock are often present in the coupled Sun-Earth plasma

system. A number of studies have suggested the formation of hot flow anomalies due to the interaction of the bow shock with an interplanetary TD or RD (e.g., Eastwood et al., 2008; Facskó et al., 2008; Lin, 1997, 2002; Maynard et al., 2002; Omidi et al., 2013, 2014; Paschmann et al., 1988; Schwartz, 1995; Schwartz et al., 1988; Sibeck et al., 2002; Thomsen et al., 1986, 1988). Another type of the interaction is magnetic reconnection between the interplanetary magnetic field (IMF) lines on the two sides of a DD in the magnetosheath (Lin, 1997; Maynard et al., 2001, 2002; Omidi et al., 2009; Phan et al., 2007, 2011). Using Cluster spacecraft observations, Phan et al. (2007, 2011) and Hasegawa et al. (2012) have identified the initiation of magnetosheath reconnection due to compression of a solar wind current sheet at the bow shock and against the dayside magnetopause. The observation event of Phan et al. (2007) has been simulated by performing a two-dimensional (2-D; Omidi et al., 2009) and a three-dimensional (3-D) global hybrid simulation (Pang et al., 2010) for the generation and structure of magnetosheath reconnection due to the interaction between an interplanetary TD and the Q-⊥ bow shock.

Magnetic reconnection (Birn et al., 2001; Biskamp, 2000; Dungey, 1961; Fu et al., 2006), associated with a rapid change of the magnetic field topology, is a fundamental plasma process that leads to an explosively conversion of magnetic energy to kinetic and thermal energy. Numerous reconnection events are reported in the interplanetary plasma space by in situ observations (e.g., Angelopoulos et al., 2008; Ashour-Abdalla et al., 2011; Gosling et al., 2005; Nagai et al., 1998, 2001; Phan et al., 2000; Retinò, Sundkvist et al., 2007; Russell & Elphic, 1979). Observations by multiple spacecraft indicate the presence of long reconnection X line in the solar wind, extending at least several million kilometers and lasting over periods of several hours (Davis et al., 2006; Gosling et al., 2005; Gosling, Eriksson, Blush et al., 2007; Gosling, Eriksson, McComas et al., 2007; Osman et al., 2014; Phan et al., 2006). Reconnection at the Earth's magnetopause is believed to be a dominant process by which the solar wind energy enters the magnetosphere, before subsequently dissipated by magnetic storms and aurorae (Burch et al., 2016; Hasegawa et al., 2010; Mozer et al., 2002; Paschmann et al., 1979; Phan et al., 2004; Wang et al., 2017). The magnetotail transient dynamics, such as bursty bulk flows, dipolarization front, flux ropes, waves, and magnetospheric substorms, are also closely related to magnetic reconnection (e.g., Angelopoulos et al., 2008; Eastwood et al., 2005; Huang et al., 2015; Lu et al., 2016; Nagai et al., 2001; Nakamura et al., 2006; Øieroset et al., 2001; Retinò et al., 2008; Wang et al., 2016; Wu et al., 2013). Evidence of reconnection in the turbulent flows downstream from the Q-|| bow shock has also been reported (Retinò, Sundkvist et al., 2007; Retinò, Vaivads et al., 2007; Yordanova et al., 2016). All the above observations indicate that magnetic reconnection is a widespread phenomenon and plays vital roles in the solar-terrestrial space.

However, the physical process of reconnection formed in the dayside magnetosheath due to interaction of an interplanetary TD with the Earth's magnetosphere is still poorly understood. The evolution of magnetosheath reconnection and the magnetic flux ropes is closely related to the paraboloidal-like bow shock and magnetopause. A 3-D model is thus necessary to investigate the 3-D features of the reconnection process in the magnetosheath. In the previous 3-D global hybrid simulation of Pang et al. (2010), two-step compression processes (shock and convective compression) in the transmitted TD is found across the Q-⊥ shock, and magnetosheath reconnection is seen to occur in current sheet downstream of the Q-⊥ shock. The simulation of Pang et al. (2010), however, is only performed for cases with a purely northward or southward initial IMF, in which the magnetic field orientation is assumed to change by 180° across the TD.

In this paper, we perform a systematic 3-D global-scale hybrid simulation to investigate the magnetosheath reconnection due to the impact of an interplanetary oblique TD. Cases with various rotation angles and initial half widths are presented in order to understand the detail physical processes of the generation, structure, evolution, and spatial distribution of magnetosheath reconnection downstream of both Q-⊥ and Q-|| shocks, due to interaction of the oblique TDs with the bow shock and Earth's magnetosphere. The interaction of the magnetosheath flux ropes with the magnetopause is also examined.

This manuscript is organized as follows. The simulation model is described in section 2. The simulation results are presented in section 3, and the summary and discussion are given in section 4.

2. Simulation Model

Numerical simulation based on a 3-D global-scale dayside hybrid code (Lin & Wang, 2005) is performed in this study. The geocentric solar-magnetospheric (GSM) coordinate is used, in which the *x* axis points from the

Earth to the Sun, and the positive z axis points to the northern magnetic pole. The y axis is defined to be perpendicular to the Earth's magnetic dipole from dawn to dusk. In the simulation, the density scaled by the ion number density n_0 in the solar wind and the magnetic field is expressed in units of the IMF strength $B_0 \sim 10nT$, corresponding to the ion gyrofrequency $\Omega_{i0} \sim 1.0s$, where $\Omega_{i0} = eB_0/m_i$ is the ion cyclotron frequency in the solar wind, e is the electron charge, and m_i is the proton mass. In the simulation, the time t is normalized to Ω_{i0}^{-1}, and the length is in units of the ion inertial length $d_{i0} = c/\omega_{pi0}$ in the solar wind, and $c/\omega_{pi0} = 0.1R_E$ is chosen. The velocity is scaled to Alfvén speed $v_{A0} = 0.1R_E/s$ in the solar wind. The electric field in units of $v_{A0}B_0$. To illustrate the simulation results on the spatial scales of the magnetosphere, the length is scaled to the Earth radius, R_E.

The simulation domain contains the magnetosphere, magnetosheath, and bow shock in the dayside region with GSM $x > 0$, while the Earth is located at $(x, y, z) = (0, 0, 0)R_E$. A spherical coordinate system is applied, with a grid number of $n_r \times n_\theta \times n_\phi = 220 \times 114 \times 150$-$n_r \times n_\theta \times n_\phi = 320 \times 150 \times 200$. Nonuniform grids are used in the r direction, with a smaller grid size of $\Delta r = 0.05R_E$ (hence, $\Delta r = 0.5d_{i_0}$) for $r \in [9R_E, 14R_E]$ in the typical cases, that is, a higher grid resolution in the bow shock, magnetosheath, and magnetopause regions. The zenith angle θ is equal zero along the positive GSM z axis, and the azimuthal angle φ is measured from the negative GSM y axis. Note that the ion inertial length in the dayside magnetosheath is around $0.05R_E \sim 0.07R_E$, and this spatial resolution used is sufficient to resolve the ion kinetic physics around the dayside magnetosheath. The time step is $\Delta t = 0.05\Omega_i^{-1}$. In the interested regions of the solar wind, magnetosheath, and magnetopause, about 150–600 particles are used in each grid cell. The simulation region is set with the range of $3.5R_E \le r \le 23R_E$. Outflow boundary conditions are used at $\theta = 0°$ and 180°, while a constant inflow boundary condition of the solar wind and IMF is applied at $r = 23R_E$. The ideally conducting condition is applied on the inner boundary at $r = 3.5R_E$.

Initially, the Earth's dipole magnetic field is imposed in $r \le 10R_E$, which interacts with the uniform solar wind and IMF in $r > 10R_E$. The solar wind flows along the $-x$ direction with an Alfven Mach number of $M_A = 5.6$. The bow shock, the magnetosheath, and magnetopause are formed in a self-consistent manner.

In this model, ions are treated as fully kinetic Vlasov particles, and electrons are treated as a massless fluid. Physical phenomena occur on the ion inertial or Larmor radius scale are resolved by such hybrid simulation. The standard particle-in-cell treatment is used to advance the ions. In our model, the equation for ion (assumed to be protons only) particle motion, in the simulation units, is given by

$$\frac{dv_p}{dt} = E + v_p \times B - \nu(u_p - u_e), \tag{1}$$

where B is the magnetic field, E is the electric field, and v_p, u_p, and u_e are the ion particle velocity and the bulk flow velocities of ions and electrons, respectively. A collision frequency, $\nu \approx 0.02\Omega_i J/J_0$, is applied to the ion bulk flow with respect to the electron fluid. Such term is imposed to simulate the ad hoc anomalous resistivity between the ions and electrons. Here Ω_i is the local ion gyrofrequency, $J_0 = B_0/\alpha d_{i0}$, and $\alpha = \mu_0 e^2/m_i$.

The E is obtained from the electron momentum equation

$$E = -u_e \times B - \nu(u_e - u_i) - \frac{\nabla P_e}{n}, \tag{2}$$

where

$$u_i = \frac{n_p}{n} u_p + \frac{n_f}{n} u_f, \tag{3}$$

from Ampere's law

$$u_e = u_i - \frac{\nabla \times B}{\alpha n}, \tag{4}$$

and P_e is the electron thermal pressure. In equation (3), discrete particles and a cold ion fluid are identified by the subscripts p and f, respectively, and $n = n_f + n_p$ is the total ion number density, or the electron density based on the assumption of quasi-charge neutrality. The n_f is given as

Table 1
Simulation Cases Presented in This Paper, With the Various Rotation Angles $\Delta\Phi$ and Initial Half Width w of the Tangential Discontinuity in the Solar Wind

Case	$\Delta\Phi(^\circ)$	$w(d_{i0})$
1	180	10
2	180	30
3	150	10
4	120	10
5	90	10
6	90	2

Note. d_{i0} is the ion skin depth in the solar wind.

$$n_f = n_{eq}[1 - \tanh(r - 6.5)]/r^3, \quad (5)$$

which is imposed in the inner magnetosphere (Swift, 1996), and r is in units of R_E. It should be noted that the ion inertial length (or the ion skin depth) can be calculated by $(\alpha n)^{-\frac{1}{2}}$ equation. The magnetic field B is updated by Faraday's law:

$$\frac{\partial \mathbf{B}}{\partial t} = -\nabla \times \mathbf{E}. \quad (6)$$

Subcycling time steps are used to advance the magnetic field, which is particularly important for the dipole-like high-field region (Swift, 1996). In our simulation, 10 time steps are used to update the magnetic field for each particle time step.The initial IMF is assumed to be $(B_x, B_y, B_z) = (-0.5, 0.0, 0.866)B_0$ in the case shown in this paper, which is in the xz plane, with an oblique angle of 30° relative to the z axis. An interplanetary TD convects earthward with the solar wind flow along the $-x$ direction. Initially, the TD front is located at a distance corresponding to $x = 36.0R_E$ where $z = 0.0R_E$, outside the simulation domain. The magnetic field across the TD, with the zero normal component of the magnetic field $B_n = 0$, is described by

$$\begin{aligned} B_x &= -\frac{1}{2}B_0 \cos[\varphi(x,z)] \\ B_y &= -B_0 \sin[\varphi(x,z)] \\ B_z &= \frac{\sqrt{3}}{2}B_0 \cos[\varphi(x,z)], \end{aligned} \quad (7)$$

$$\varphi(x,z) = \Delta\Phi\left(1 + \tanh\left(\frac{\sqrt{3}(x - x_{TD}(z,t))}{2w}\right)\right)/2, \quad (8)$$

where $x_{TD}(z,t) = 36 - \frac{\sqrt{3}}{3}z - v_0 t$ is the x position of the TD center as a function of time t and position z, v_0 is the solar wind flow speed, and $\Delta\Phi$and w are the rotation angles of the tangential magnetic field and initial half width of the TD, respectively. The initial TD possesses a circularly polarized magnetic field, which is described by equations (7) and (8). Cases with $\Delta\Phi = 90°$–$180°$ and $w = 2d_{i0}$–$30d_{i0}$ are presented. For the case with $w = 2d_{i0}$, a higher grid resolution with $\Delta r = 0.025R_E$ is used.

In the following, we show six cases with various rotation angles $\Delta\Phi$ and initial half width w, as listed in Table 1. We first show a case with $\Delta\Phi = 180°$ and $w = 10d_{i0}$ in detail, and then discussion effects of w and $\Delta\Phi$.

3. Simulations Results

3.1. Case 1: $\Delta\Phi = 180°$ and $w = 10d_{i0}$

As described in section 2, initially, the interplanetary TD front is located at a distance corresponding to $x = 36.0R_E$ where $z = 0.0R_E$, outside the simulation domain. The interplanetary TD convects earthward with the solar wind flow velocity along the $-x$ direction. It first reaches the outer boundary at about $t = 14.0$, and then enters the simulation domain. The magnetic field on the outer hemispherical boundary changes in response to the arrival of the TD at each specific point, as described by equations (7) and (8). Figure 1 shows a close-up of the magnetic field in the noon-meridian plane and some magnetic field lines at $t = 30.0$ obtained in case 1, in which $w = 10d_{i0}$, or $1R_E$. Two colors of the field lines are shown in this figure, with the black ones are the closed dipole field lines and yellow ones representing the interplanetary field lines. Over the curved shock front, under a specific IMF direction, the shock normal angle $\theta_{Bn} > 45°$ ($<45°$) corresponds to the Q-$\perp$ (Q-$\parallel$) shocks. In this case, the IMF changes by angle $\Delta\Phi = 180°$, from $(B_x, B_y, B_z) = (-0.5, 0.0, 0.866)B_0$ ahead of the discontinuity to $(B_x, B_y, B_z) = (0.5, 0.0, -0.866)B_0$ on the sunward side of the incoming TD. So the angle $\theta_{Bn} > 45°$ exits where $z > -3.5R_E$ at the bow shock, corresponding to the quasi-perpendicular shock. In $z < -3.5R_E$, the angle $\theta_{Bn} < 45°$, which is a quasi-parallel shock. The bow shock front is fully formed by $t = 25.0$, and the incoming TD first touches the Q-$\perp$ shock around $t = 35.0$. The structure of the TD remains nearly unchanged before it reaches the Q-$\perp$ shock.

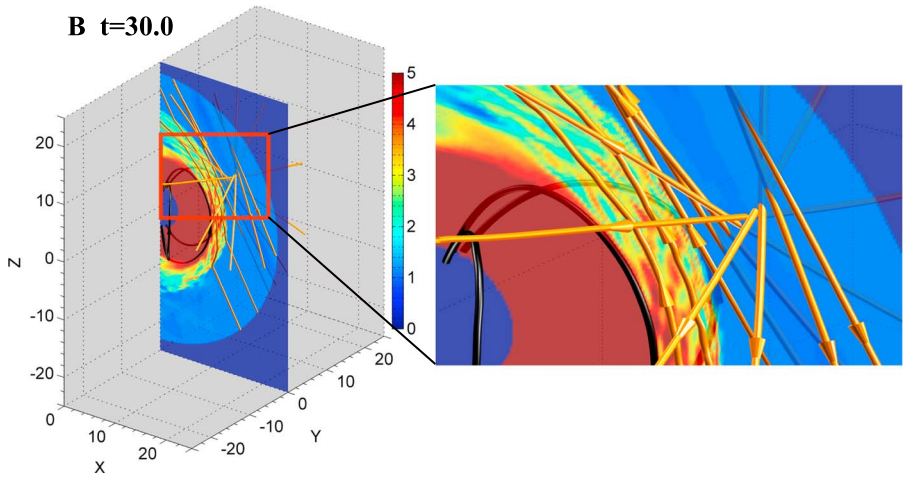

Figure 1. (left) Contours of the magnetic field strength in the noon meridian plane at t = 30.0 obtained from case 1. The black lines are the closed geomagnetic field lines (tubes) in 3-D perspectives, and the yellow lines are the open interplanetary field lines, including those in the incident interplanetary tangential discontinuity with field direction angle $\Delta\Phi = 180°$. The tangential discontinuity is still in the upstream and yet to reach the bow shock at t = 35.0. (right) A zoom-in view.

When the planar TD reaches the bow shock, it first encounters the area where the IMF is tangential to the shock front, that is, the perpendicular shock. Due to the nonuniform spatial distribution of physical quantities, the TD undergoes different degrees of slowing down at different locations, and thus distorts when passing through the bow shock toward the magnetopause. Meanwhile, the TD is dragged tailward by the solar wind, forming a paraboloidal-shaped structure. In this case, the TD nearly passes through the Q-⊥ bow shock in the simulation domain at t = 40.0, and the average half width of the transmitted TD has been compressed to about 0.25 R_E, (approximately one fourth of the initial width of the TD in the solar wind), about $2.5d_{i0}$ or $4.25d_i$, by the shock compression at the Q-⊥ bow shock, where d_i is the ion inertial length in the local magnetosheath. When the transmitted TD is moving against the magnetopause, the second-step, convective compression further reduces the width of the transmitted TD. Such two-step compression processes have also been described in a previous simulation study by Pang et al. (2010).

Magnetic reconnection is found to take place in the center of the transmitted TD around t = 45.0 downstream of the Q-⊥ shock. The magnetic field configuration and characteristics of particle acceleration can be used to identify the occurrence of magnetic reconnection, as discussed below. Figures 2a–2d show contours of the magnetic field strength, ion density, and the B_y component of magnetic field in the meridian plane, as well as the field lines around a zoomed-in region of the transmitted TD downstream of the Q-⊥ shock, respectively, at t = 60.0. The positions of the magnetopause and bow shock can be identified by the sudden gradients of the magnetic field strength and ion density around x = $10.0R_E$ and $14.0R_E$ around the subsolar area in Figures 2a and 2b, respectively. Also shown in Figures 2c and 2d are the typical magnetic field lines, with the red ones and black ones being associated with the Q-⊥ bow shock and the magnetopause, respectively. The orange lines, one the other hand, reveal the field lines downstream of the bow shock that have gone through a topology change through magnetosheath reconnection. The white ones in the zoomed Figure 2d represent the open magnetosheath field lines just outside the magnetosheath merging layer, and the green ones are for the reconnected field lines near the X line. The average width of the transmitted TD has been further compressed when it continues to move earthward so that the magnetic field pileup against the magnetopause. At t = 60.0, magnetic flux ropes are present mainly at four locations, as shown by the magnetic field configuration in Figure 2c, centered around z= 2.2, 4.7, 8.2, and 11.3 R_E downstream of the Q-⊥shock, about $1.5R_E$ away from the magnetopause. These magnetic flux ropes can be viewed as time-dependent reconnection events due to localized multiple X lines, which extend in the dawn-dusk direction over the dayside magnetosheath region downstream of the Q-⊥ bow shock. At the center of the flux ropes, the magnetic field strength and the B_y component appear to be relatively strong, as shown in Figures 2a and 2c, and the ion density is also fairly dense as shown in Figure 2b. Two flux ropes, marked by "D" and "E" (to be discussed further in Figure 7),

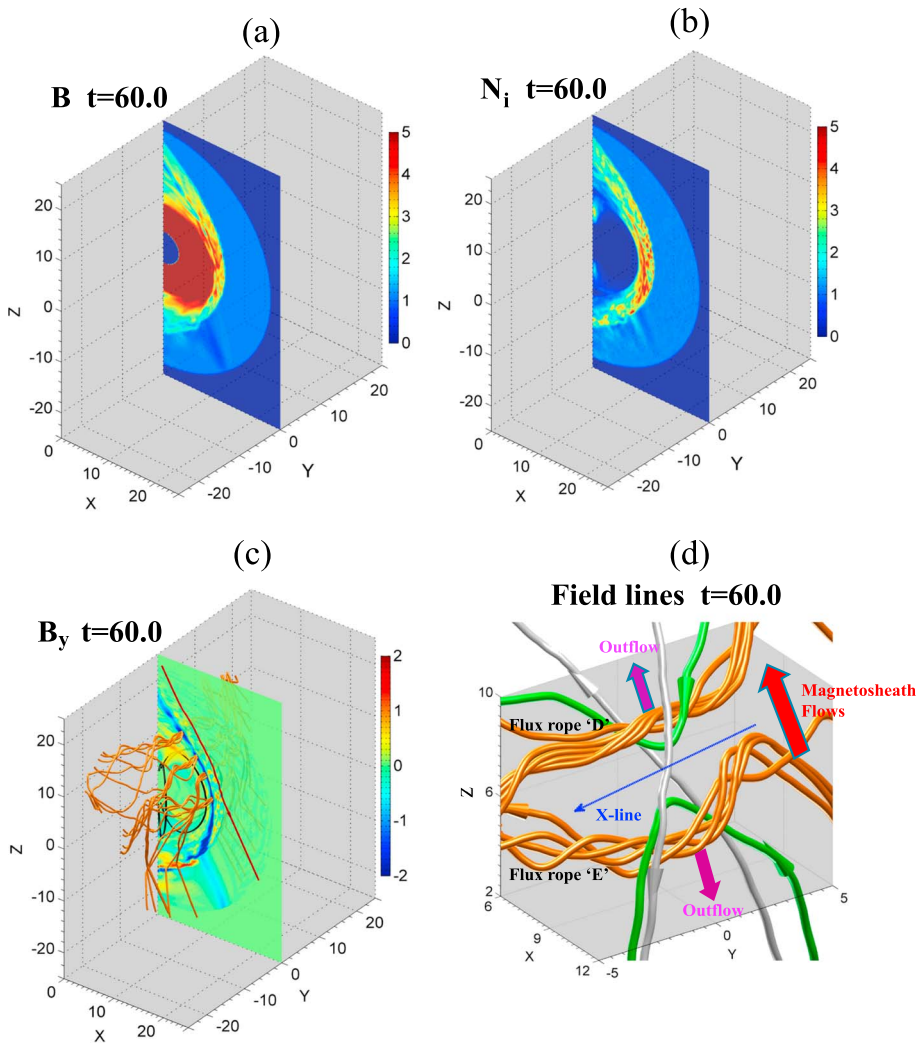

Figure 2. Contours of the (a) magnetic field strength B, (b) ion number density N_i, (c) the B_y component of magnetic field in the noon meridian plane at t = 60.0 obtained, and (d) some field lines around the transmitted tangential discontinuity downstream of the Q-⊥ shock at t = 60.0 in case 1. Superposed on the B_y contours are some typical magnetic field lines, with the red and black ones being those around the Q-⊥ bow shock and at the magnetopause, respectively. The yellow lines are the field lines reconnected in the magnetosheath. The white lines represent open magnetic field lines outside the magnetosheath merging layer, the green lines are the reconnected field lines inside the merging layer, and the blue dotted line denotes the corresponding X-line. The red arrow indicates magnetosheath flow direction, and the violet arrows in the plots of field lines mark the reconnection outflows.

are highlighted in Figure 2d. Between the ropes "D" and "E" centered around z= 4.7 R_E and 8.2 R_E, respectively, at t = 60.0 there exists an X-line, marked by the blue dotted line. The magnetosheath flows are almost pointing northward, as marked by the red arrow in Figure 2d. Plasma outflows also appear near the reconnection X point, as sketched by the violet arrows in Figure 2d.

Detailed structures of various physical quantities around the flux ropes "D" and "E" (indicated in Figure 3c) are shown in Figure 3, which depicts the zoomed-in contours of the magnetic field B, B_x, B_y, and B_z; ion number density N_i; electric field E_x, E_y, and E_z; ion temperature $T_{\parallel}$ and $T_{\perp}$; ion bulk flow V_x, V_y, and V_z; and current density j_x, j_y, and j_z in the noon meridian plane (y = 0), from x = 6.0R_E to 12.0R_E and from z = 2.0R_E to 10.0R_E at t = 60.0. The bow shock can be seen at a standoff distance of r = 14.0R_E, across which B, N_i, and the $T_{\perp}$ increase in the antisunward direction (see Figures 3a, 3e, and 3m). The increase (decrease) in B (N_i) through the standoff distance of r = 10.0R_E marks the magnetopause (see Figures 3a and 3e). In Figures 3b and 3d, the transmitted current sheet can be seen where B_x and B_z field direction reverses (indicated in

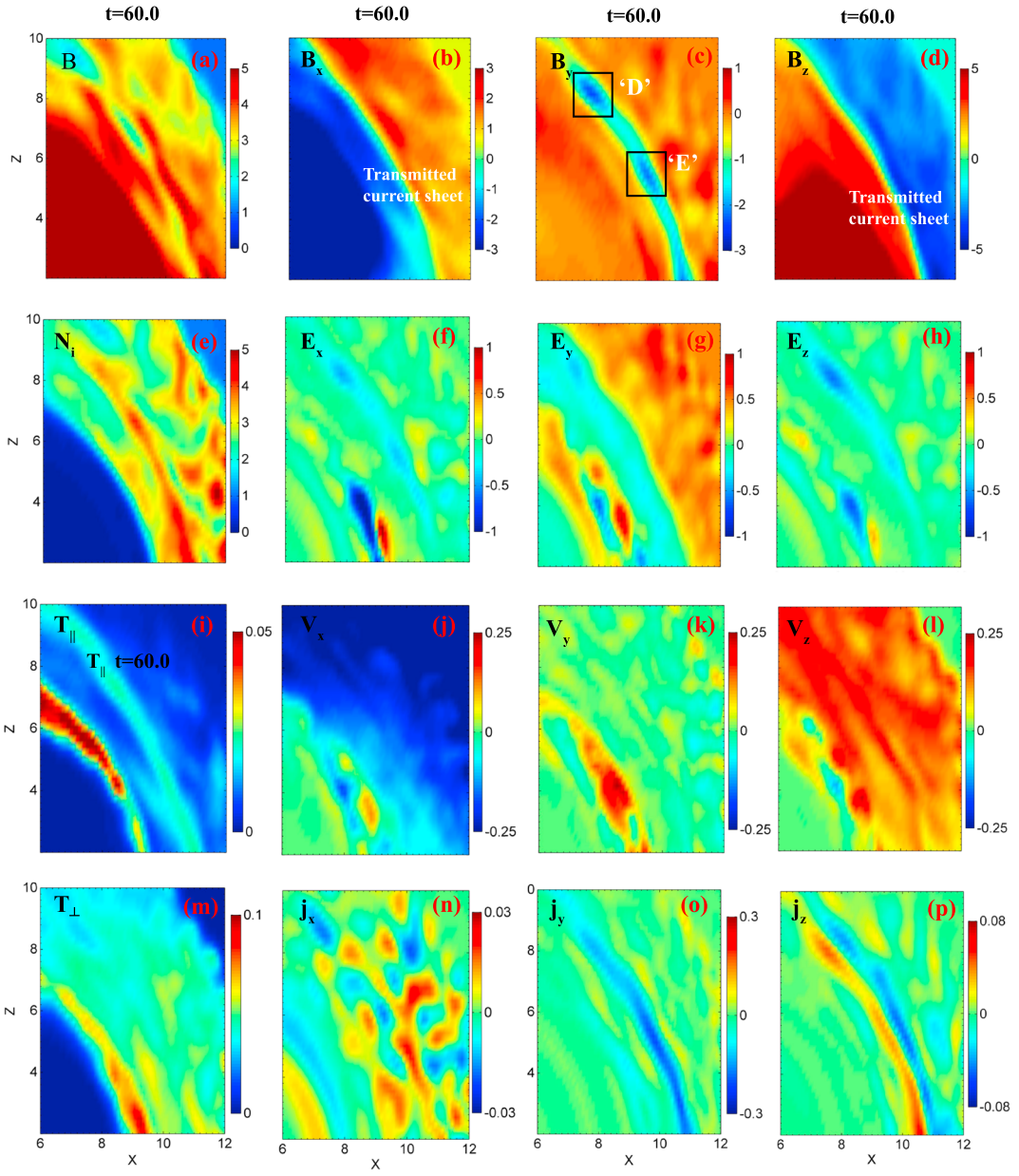

Figure 3. Zoomed-in contours of magnetic field (a) B, (b) B_x, (c) B_y, and (d) B_z; ion number density (e) N_i; electric field (f) E_x, (g) E_y, and (h) E_z; ion temperature (i) $T_{||}$ and (m) $T_\perp$; ion bulk flow (j) V_x, (k) V_y, and (l) V_z; and current density (n) j_x, (o) j_y, and (p) j_z around the flux ropes "D" and "E" in region $x \in [6.0, 12.0]R_E$ and $z \in [2.0, 10.0]R_E$ in the noon meridian plane, at $t = 60.0$.

Figure 3), and the half width of the current sheet is about from $3.5d_i$ to $5.5d_i$. Due to the magnetopause obstacle, the magnetosheath flows convect poleward and tailward along the magnetopause, as shown in Figures 3j, 3k, and 3m. The magnetosheath reconnection has caused the formation of flux ropes "D" and "E" in the transmitted current sheet, whose center can be identified by the strong core field B_y, around $(x, z) = (7.6, 8.2)R_E$ and $(x, z) = (9.0, 4.7)R_E$ (see Figure 3c), which will be further discussed in Figure 7. At the center of the flux ropes, the magnetic field strength and ion parallel temperature appear to be relatively high, and the ion density is also fairly dense (see Figures 3a, 3e, and 3i). It is also seen from Figures 3f–3e that the electric field have a negative value around the center of the transmitted current sheet due to the effect of $-\mathbf{V} \times \mathbf{B}$. In addition, wave fluctuations of the electromagnetic fields are also present in the magnetosheath, as shown in Figures 3a, 3c, and 3f–3h. Due to the large magnetic field B_y in the incoming TD and thus the transmitted current sheet, the Hall structure of the electric and magnetic field cannot to

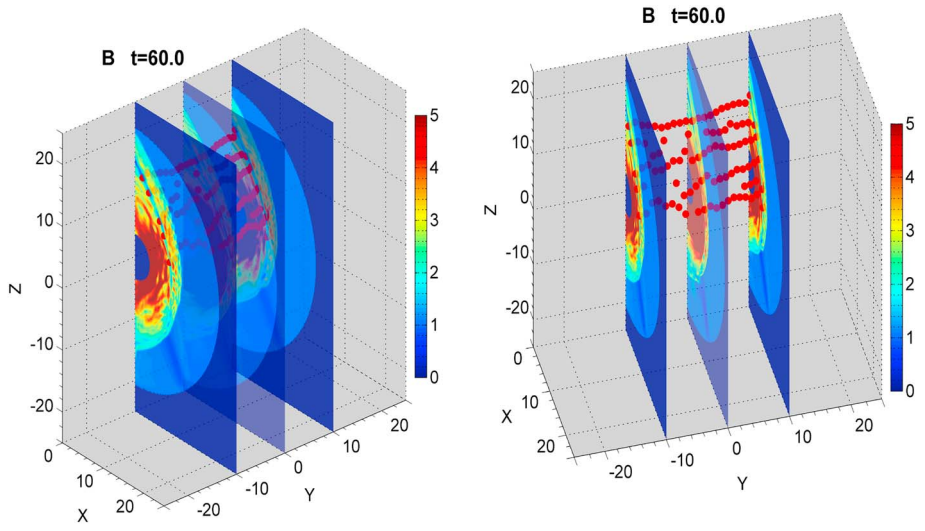

Figure 4. Contours of B at t = 60.0 in three planes at $y = -10.0$, 0, and 10.0 R_E obtained in case 1. The dots represent the relatively weak field region in various planes parallel to the noon meridian plane with an increment of $\delta y = 1R_E$ range between $y = -10R_E$ and $10R_E$, tracking the X lines.

be seen in Figure 3. More elaborations of the detailed structure of reconnection in the magnetosheath will be given in Figures 7 and 8.

In order to illustrate the size of each reconnection region in the magnetosheath, Figure 4 depicts contours of the magnetic field strength at t = 60.0 in three planes at $y = -10R_E$, 0, and 10 R_E, respectively. The red dots in Figure 4 represent the locations of relatively weak field in various planes parallel to the noon meridian plane with a increment of $\delta y = 1R_E$ between $y = -10R_E$ and $10R_E$. Magnetic reconnection is found to take place around the weak magnetic field regions, producing magnetic flux ropes in the magnetosheath, as indicated by the yellow field lines in Figure 2c. Local X points are found to exist at these weak field regions. These are the X points on a finite-length X line, which are identified by its typical magnetic field configuration and characteristics of particle acceleration. An example is shown below in Figure 9. The magnetic topology of the X points is further confirmed by using the topological degree method (Greene, 1992; Xiao et al., 2006) after subtracting the guide field component. In order to illustrate the 3-D distribution of the reconnection regions in the magnetosheath, Figure 4 is presented from two perspectives. The scale lengths of the magnetosheath flux ropes are about $1.5R_E$ in both the radial and latitudinal directions, but ranging from $y = -15.0R_E$ to $12.0R_E$ in the dawn-dusk direction (to be shown in Figure 11). It indicates that such patchy structure of reconnection is very different from that in the 2-D processes.

The process of the formation of some magnetic flux ropes in the magnetosheath is illustrated in Figure 5, which shows the contours of the magnetic field strength in the noon meridian plane at t = 50.0. Magnetic field lines inside the merging layer are also superposed on the plot, corresponding to a 3-D patchy reconnection. The red circles indicate the X points of reconnection that has been triggered, while the blue boxes denote the X points where magnetic reconnection is about to occur at t = 53.0. As a result, a new X line, marked by the white dotted line in Figure 5, is formed through the blue X points, leading to the 3-D patchy reconnection, consistent with the patchy reconnection model (Lee et al., 1993, Figure 8).

Figure 6 displays spatial profiles of the structure of magnetic reconnection in the later stage at t = 80.0 and 88.0. Four bundles of field lines (black, yellow, blue, and red) are shown in this figure. The black, red, and yellow lines are the reconnection magnetic field lines similar to those described for Figure 2, while the blue lines represent the closed and open field lines around the magnetopause. At t = 80.0, the flux ropes are more distorted as compared to the flux ropes in Figure 2, and the half width of the current sheet is approximately $1.5d_i$. The flux ropes downstream of the Q-⊥ bow shock carried by the incoming TD have touched the magnetopause, pilling up with the ambient field fluxes. Under the drag of the magnetosheath plasma flows, they also propagate poleward and tailward along the magnetopause.

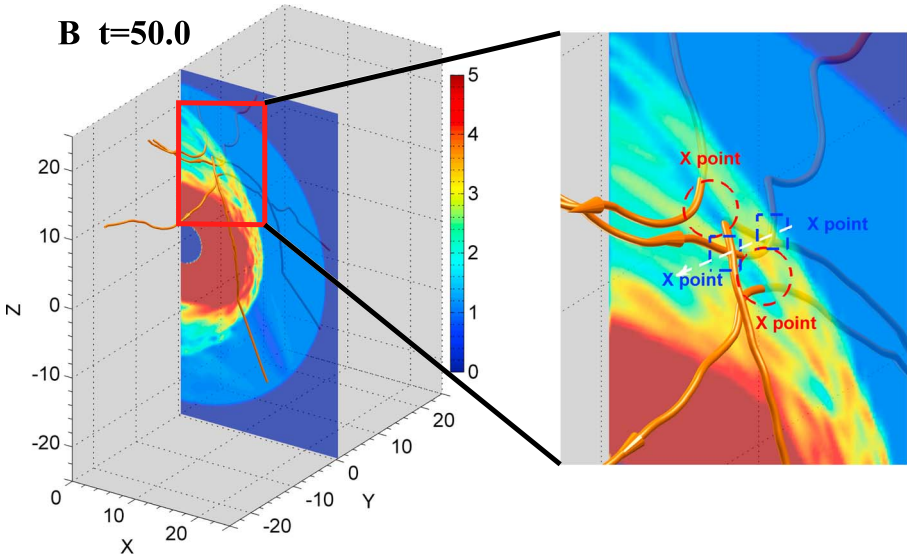

Figure 5. Contours of B in the noon meridian plane together with 3-D magnetic field lines inside the magnetosheath merging layer at t = 50.0 obtained in case 1. The red circles indicate the X points of reconnection that has been triggered. The blue boxes denote the X points of reconnection to occur at t = 53.0, and the white dotted line denotes the corresponding new X-line.

Meanwhile, reconnection flux ropes are also present downstream of the Q-|| shock, at a distance much closer to the magnetopause (about 0.7R_E) than those downstream of the Q-⊥ shock (about 3.6R_E). As shown in Figure 6, at t = 80.0 the flux ropes are obviously present near the magnetopause downstream of the Q-|| bow shock, and the length of these flux ropes in the dawn-dusk direction (10R_E) is significantly shorter than that downstream of the Q-⊥ shock (27R_E). These reconnection events are found to take place locally behind the Q-|| bow shock. Different from the process at the Q-⊥ shock, a convective compression takes the dominant role in the narrowing of this part of the transmitted TD.

At t = 88.0, magnetopause reconnection is also seen to be initiated, as shown by the blue field lines in Figure 6, indicating that the magnetic fluxes with the southward IMF (on the sunward side of the transmitted TD, antiparallel to the geomagnetic field) have reached and interacted with the magnetopause. Magnetopause flux ropes wrap and mix with the magnetosheath flux ropes. The scale lengths of the magnetosheath ropes are significantly larger than the sizes of magnetopause ropes in the dawn-dusk direction, but nearly comparable with those of the magnetopause flux ropes in both the radial and latitudinal directions.

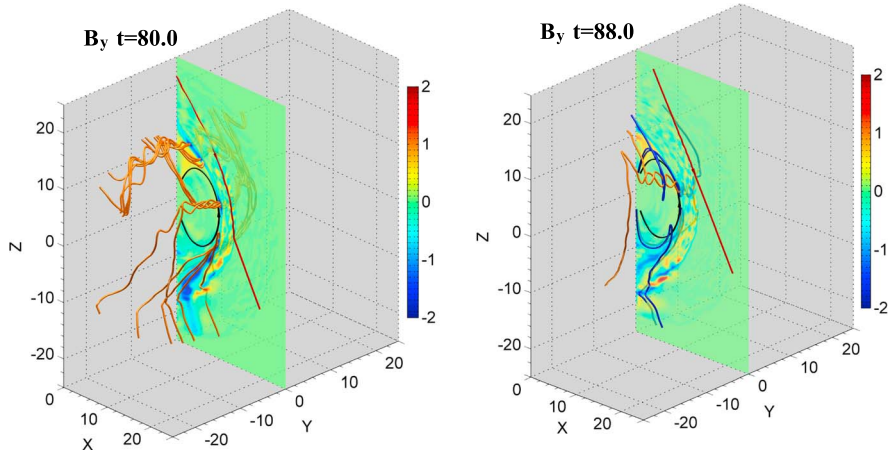

Figure 6. Contours of the B_y field in the noon meridian plane displays at t = 80.0 and 88.0, respectively, obtained in case 1. The black, red, and yellow lines are the field lines similar to those described for Figure 2, while the blue field lines represent the reconnected field lines around the magnetopause.

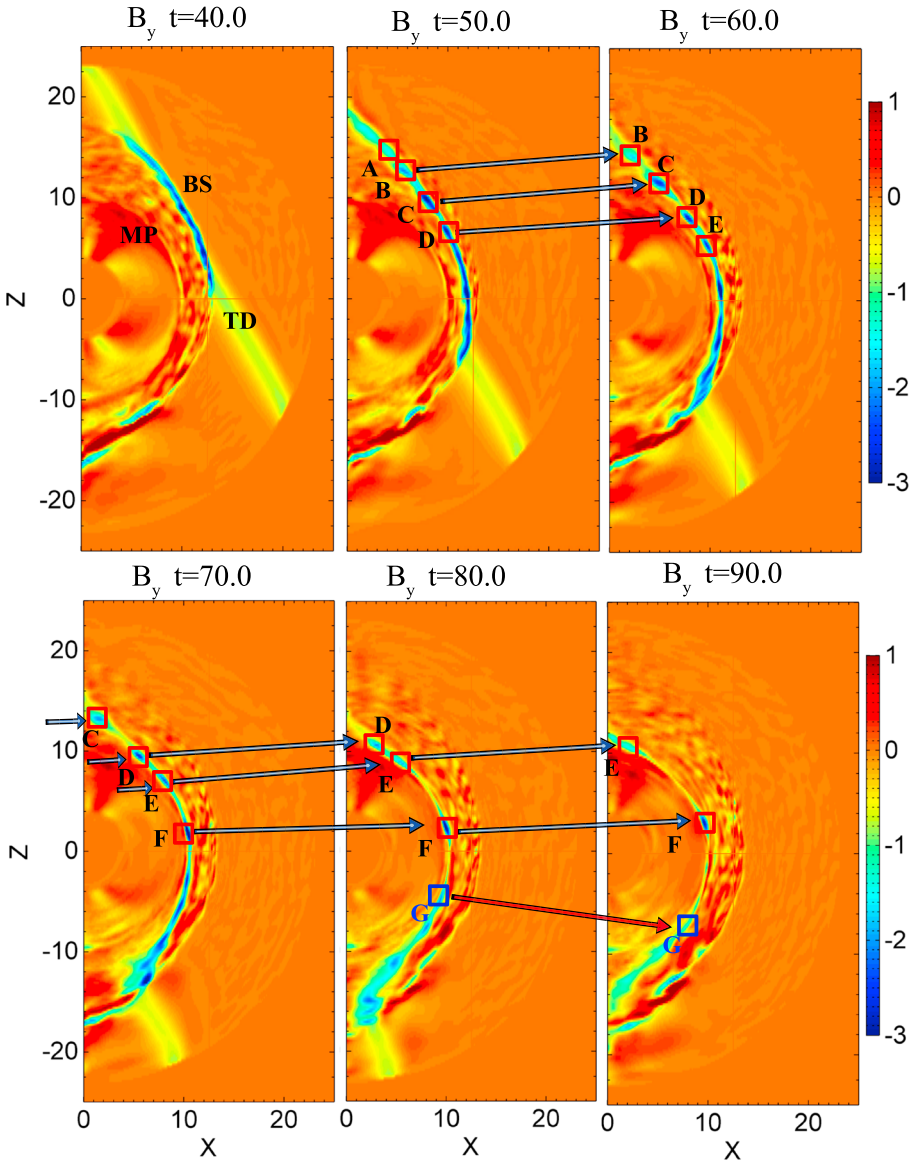

Figure 7. Contours of B_y in the noon meridian plane at t = 40.0, 50.0, 60.0, 70.0, 80.0, and 90.0, respectively, obtained in case 1. Bundles of the y-component fluxes are denoted by "A," "B," "C," "D," "E," "F," and "G." TD = tangential discontinuity; MP = magnetopause and BS=Bow Shock.

To track the time evolution of magnetic flux ropes in the magnetosheath, we show in Figure 7 the B_y field in the noon meridian plane at t = 40.0, 50.0, 60.0, 70.0, 80.0, and 90.0. Before$t$ = 35.0, B_y is nearly uniform in the center of the incident TD upstream of the shock. However, the structure of magnetic field B_y becomes highly nonuniform after the TD reaches the bow shock. At t = 40.0, the transmitted TD is significantly compressed by the bow shock when it passes through the Q-⊥ shock, and magnetic reconnection is just about to be initiated. Bundles of the y-component fluxes, denoted by "A," "B," "C," "D," "E", and "F" are formed, as seen at t = 50.0, 60.0, and 70.0. These flux ropes only appear downstream of the Q-⊥ shock. The y-component magnetic fluxes are swept out by the newly generated high-speed outflows when reconnection takes place in a certain region, leading to a local reduction of B_y. Such reduction causes a decrease in magnetic pressure and thus further narrowing down of the region. The magnetic field is locally more antiparallel-like, which is preferable for more reconnection. The subsequent reconnection produces bundles of the B_y flux shown at t = 50.0, 60.0, and 70.0. The bundles of the y-component flux that are located at $(x, z) = (10.0, 6.2)R_E$ at t = 50.0. They have moved to $(x, z) = (4.5, 10.0)R_E$ at t = 70.0, corresponding to a convection speed of nearly $3v_{A0}$, consistent

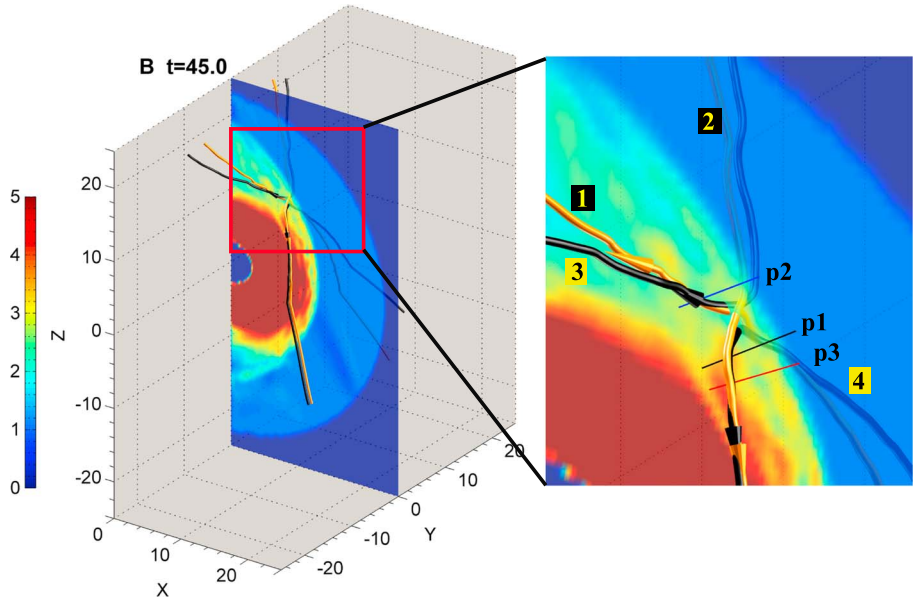

Figure 8. Contour plots of B in the noon meridian plane at t = 45.0 obtained in case 1. The yellow lines marked by "1" and "2" represent open magnetic field lines outside the magnetosheath merging layer, and the black lines denoted by "3" and "4" are the reconnected field lines around an X line inside the merging layer. The three paths, marked by p1 (southward from the X line), p2 (northward from the X line), and p3 (southward from the X line), are through reconnection regions of the transmitted current sheets.

with the corresponding flow speed in the magnetosheath. Because the shock compression is largely weakened when the TD passes through the Q-|| bow shock, the dominant narrowing mechanism of the TD there is rather though the convective compression while the TD is moving toward the magnetopause in the magnetosheath, as mentioned above. As a result, it takes more time to compress the transmitted TD to thin enough to triggering reconnection downstream of the Q-|| shock than at the Q-⊥ shock. At t = 80.0, the bundles of the y-component flux marked by "G" in Figure 7 are formed downstream of the Q-|| shock. The flux ropes formed downstream of the Q-|| shock propagate tailward and poleward along the plane of magnetopause.

The above case is similar to the event of magnetosheath reconnection observed by Phan et al. (2007). Figures 8 and 9 demonstrate the detailed structures at various distances from a magnetosheath X line. Figure 8 shows the contours of the magnetic field strength in the noon meridian plane and four field lines at t = 45.0. Two colors are shown for the field lines, with the yellow ones marked by "1" and "2" representing the open IMF lines outside the magnetosheath merging layer, and the black ones denoted by "3" and "4" for the reconnected field lines in the magnetosheath merging layer. At t = 45.0, the topology of magnetic field lines has changed rapidly inside the merging layer in the magnetosheath. For a virtual spacecraft passing through the reconnection site in an outbound direction along the colored trajectories, marked by p1 (southward from the X line), p2 (northward from the X line), and p3 (southward of the X line) in Figure 8, the spatial profiles of the magnetic field and plasma quantities detected by this probe are shown in the left, middle, and right column, respectively, in Figure 9.

The central region of the reconnection current sheets (or transmitted TDs) is bounded by two vertical black dotted-dashed lines in Figure 9. A dip of the magnetic field strength is found in the center of the current sheets in Figures 9a(1)–9a(3) (Behannon et al., 1981), which are denoted by the vertical red dotted lines. The magnetic field and ion bulk velocity are shown in Figures 9b(1)–9b(3) (Behannon et al., 1981) and 9d(1)–9d(3) (Behannon et al., 1981), respectively, in the LMN coordinates, which are determined by the Minimum Variance Analysis technology, where L is along the antiparallel magnetic field direction, M is along the X-line (approximately the y direction), and N is along the current sheet normal direction.

Along path p1 southward of the X point, the B_L component reverses the direction across the current sheet, while the normal component B_N remain to be a small constant. The B_M component appears to be a shifted quadruple structure (associated with the Hall effects) in a slightly asymmetric current layer, which has a

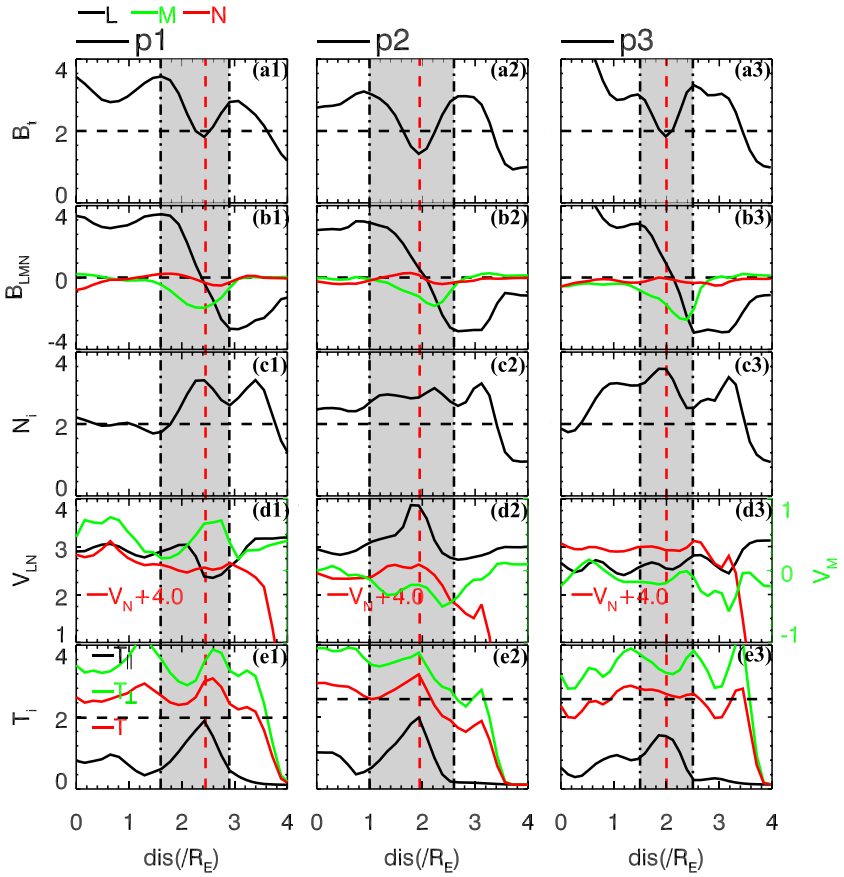

Figure 9. Spatial profiles of (a1–a3) the field strength B, (b1–b3) field components B_L (black), B_M (green), and B_N (red) in the LMN coordinate system, (c1–c3) ion number density, (d1–d3) ion bulk flows in the LMN coordinates, (e1–e3) ion temperatures $T_{\|}$ (black) and $T_{\perp}$ (green), and the total ion temperature T (red) in the outbound direction along paths p1 (left column), p2(middle column), and p3 (right column) in Figure 8. The two-vertical black dotted-dashed lines bound the central reconnection region of the transmitted tangential discontinuity. The magnetic field strength shows a dip in the center of the reconnection current sheet, as denoted by a vertical red dotted line.

width of approximately 16.0d_i. Although in our simulation the initial solar wind condition is slightly different from the observation (Phan et al., 2007; the normal of the solar wind discontinuity in their observation is along the GSE direction [0.93, −0.06, −0.36]), these simulated features of the structure of reconnection are consistent with the observed magnetosheath reconnection events (Phan et al., 2007).

At this location p1 above the equator, the ambient magnetosheath flow V_L is northward (positive). However, the tangential flow component V_L in Figure 9d (Angelopoulos et al., 2008) shows a southward acceleration in the center of the reconnection current sheet due to the existence of an X point northward of the virtual spacecraft location. Such accelerated ion flow in V_L is nearly equal to 70km/s, and the width of outflow is approximately 10.0d_i, very close to the observation results (Phan et al., 2007). In addition, nearly constant value of V_M and V_N are present in the reconnection layer. The normal component V_N has a large negative value upstream of the bow shock due to the incoming solar wind. There is also a corresponding increase in the ion density, as shown in Figure 9c (Angelopoulos et al., 2008). The enhancements in the density and the parallel and total ion temperatures (Figure 9e; Angelopoulos et al., 2008) are closely correlated with the flow ejection at the center of the current sheet, also consistent with the observation results (Phan et al., 2007) and a previous simulation results (Pang et al., 2010).

Along path p2 northward of the X line, the tangential flow component V_L in Figure 9d (Ashour-Abdalla et al., 2011) shows a northward enhancement in the reconnection current layer, opposite to the V_L profile along path p1. Such change in V_L is equal to about 80km/s. The structures of other physical quantities are similar to those along path p1. We have also selected a path p3, southward of the X point but at a father distance

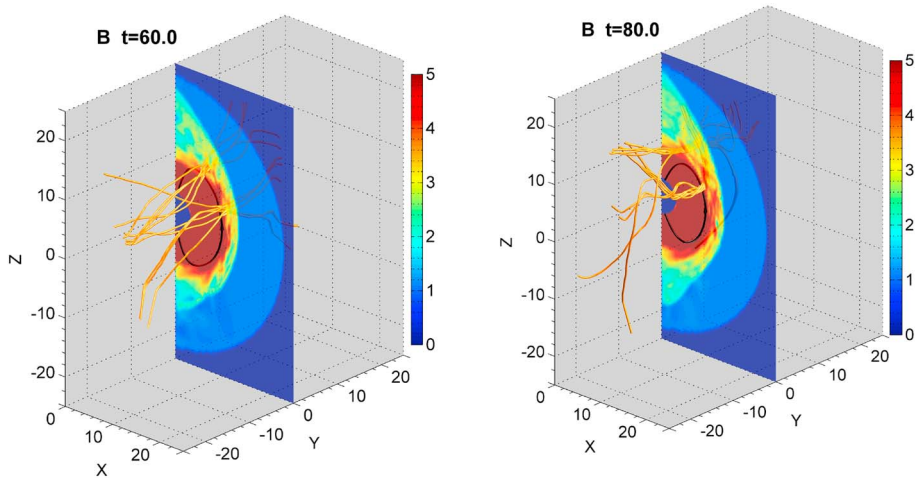

Figure 10. Contours of B_y in the noon meridian plane obtained at t = 60.0 and 80.0 in case 2. Also shown are some magnetic field lines, with the black and yellow lines showing the field lines at the magnetopause and in the magnetosheath, respectively.

than location p1. The spatial structures of magnetic field, ion density, and ion temperature at p3 are consistent with those along path p1, but there appears to be very small change in the ion flow component V_L, as shown in Figure 9d (Behannon et al., 1981). The reason for the lack of acceleration is due to the existence of another X line closeby, just southward of the virtual spacecraft location p3.

3.2. Case 2: $\Delta\Phi = 180°$ and $w = 30d_{i0}$

With a thicker initial width of the TD in the solar wind, the evolution of the TD is different as compared with that in case 1 with a relatively thin TD. Figure 10 shows the contours of B_y in the noon meridian plane obtained at t = 60.0 and 80.0 for case 2, which is similar to case 1 but with a larger $w = 30d_{i0}$, or $3R_E$. Superposed on the B_y plots are the magnetic field lines, with the black and yellow ones being the field lines at the magnetopause and the magnetosheath, respectively. In contrast to case 1, magnetic flux ropes are not obviously formed at t = 60.0. Later at t = 80.0, flux ropes are formed, as seen from the magnetic field configuration of 3-D patchy reconnection downstream of the Q-⊥bow shock. For a thin solar wind TD, it is possible the bow shock compression alone can trigger reconnection downstream of the Q-⊥ shock. If the initial TD is thick, however, a second-step (i.e., convective) compression appears to be necessary for the occurrence of reconnection. As a consequence, it takes more time to form the magnetosheath reconnection in case 2 than in case 1. However, the magnetic flux ropes cannot be found downstream of the Q-|| shock.

3.3. Cases 3–7 With Varies Rotation Angles $\Delta\Phi$

We now discuss the structure of magnetic flux ropes formed in the magnetosheath for solar wind TDs with different rotation angles, assuming $w = 10d_{i0}$. In case 3 with rotation angle $\Delta\Phi = 150°$, the reconnection flux ropes are formed around t = 42.0 at the Q-⊥ shock, nearly same time as that in case 1 ($\Delta\Phi = 180°$). They are also seen downstream of the Q-|| shock, at about t = 82.0, later than the corresponding time (t = 76.0) for case 1. When the rotation angle of the transmitted TD decreases to $\Delta\Phi = 120°$, in case 4, the flux ropes are formed at the Q-⊥ shock around t = 46.0, later than that in cases 1 and 3, whereas no flux ropes are found downstream of the Q-|| shock during the entire time when the transmitted TD passes through the magnetopause.

Figure 11 shows the contours of B in various planes that are parallel to the noon meridian plane obtained at t = 60.0 for cases with the rotation angles with $\Delta\Phi = 120°$, 150°, to 180° in the solar wind. The yellow field lines denote the reconnection flux ropes downstream of the Q-⊥ shock. It is found that the extent of the magnetic flux ropes varies with $\Delta\Phi$, as summarized in Table 2. The magnetic flux ropes are present within the region from $y = -9.0R_E$ to $3.5R_E$ for rotation angle $\Delta\Phi = 120°$ in case 4, from $y = -10.0R_E$ to $5.0R_E$ for $\Delta\Phi = 150°$ in case 3, and from $y = -15.0R_E$ to $12.0R_E$ for $\Delta\Phi = 180°$ in case 1. Our results indicate a longer length of magnetic flux ropes under a larger rotation angle $\Delta\Phi$. Moreover, there exists a dawn-dusk asymmetry in the spatial extent of the magnetosheath flux ropes. As the rotation angle $\Delta\Phi$ decreases, the dawn-dusk asymmetry of the flux ropes becomes more significant.

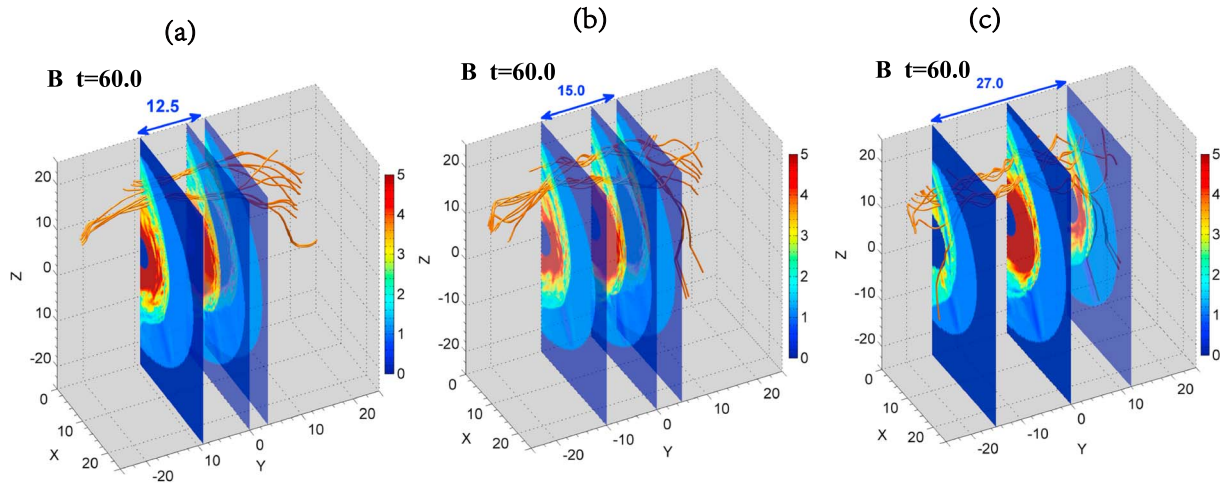

Figure 11. Contours of B in various planes parallel to the noon meridian plane obtained at t = 60.0 for (a) $\Delta\Phi$ = 120° (case 4), (b) 150° (case 3), and (c) 180° (case 1). Superposed on the contours are the field lines inside the magnetosheath merging layer. The yellow field lines denote the reconnection flux ropes.

When the rotation angle of the transmitted TD decreases to $\Delta\Phi$ = 90°, the reconnection flux ropes cannot be found in the magnetosheath. Figure 12 shows the contours of B in the noon meridian plane obtained at t = 60.0 for case 5 with $\Delta\Phi$ = 90° in the solar wind. Superposed on the contours are the magnetic field lines, with the black ones being around the magnetopause, the orange lines revealing the field lines of the transmitted TD in the magnetosheath, and the red lines being the field lines in the solar wind. In contrast to the above cases with the rotation angles of $\Delta\Phi$ = 120°, 150°=, to 180°, reconnection flux ropes are not formed in the magnetosheath at t = 60.0. The simulation is run till t = 90.0 when the transmitted TD has passed into or through the magnetopause, and no magnetosheath reconnection flux ropes are found in the entire run. We have also run case 6 with $w = 2d_{i0}$, till t = 90.0. Again, no magnetosheath reconnection is found in the transmitted current sheet. Note that previously based on a 2-D hybrid simulation, Lin (1997) has found that there is little magnetic reconnection in the magnetosheath if the rotation angle is less than 80°.

4. Summary and Discussion

In this paper, we have presented results of a systematic 3-D global hybrid simulation to investigate the interaction of a circularly polarized interplanetary TD with the bow shock, magnetosheath, and magnetopause. The main results are summarized below.

(1). As the TD is transmitted first through the Q-⊥ shock and then the Q-|| shock regions, magnetosheath reconnection may be found downstream of both the Q-⊥ and Q-|| shocks. The transmitted TD is narrowed by different compression processes at the two types of shocks. Through the Q-⊥ shock, the width of TD becomes thinner by the shock compression and convective compression process. The 3-D patchy reconnection is initiated first in the transmitted, thinned TD downstream of the Q-⊥ shock, forming flux ropes in the magnetosheath. These processes downstream Q-⊥ shock are also consistent with the simulation results of Pang et al. (2010).

(2). As the TD passes through the Q-|| shock, the shock compression is largely weakened, and the convective compression takes the dominant role in the narrowing of the TD current sheet. A longer time is necessary to compress the transmitted TD to thin enough in order to trigger the 3-D patchy magnetic reconnection downstream of the Q-|| shock. In the cases in which magnetic reconnection are also triggered downstream of the Q-|| shock, the flux ropes downstream of the Q-|| shock starts to form at a distance much closer to the magnetopause than those downstream of the Q-⊥ shock, and the length of these flux ropes is significantly shorter than that downstream of the Q-⊥ shock. For example, the flux ropes starts to form at a distance of 0.7R_E (3.6R_E)

Table 2
Extent of the Resulting Magnetosheath Magnetic Flux Ropes in the Dawn-Dusk Direction Under Various Field Rotation Angles ΔΦ From 120° to 180° Across the Tangential Discontinuity in the Solar Wind

$\Delta\Phi(^\circ)$	$y_-(R_E)$	$y_+(R_E)$	$L(R_E)$
120	−9.0	3.5	12.5
150	−10.0	5.0	15.0
180	−15.0	12.0	27.0

Note. The dawn-side and dusk-side boundary locations of the flux ropes are denoted by y_- and y_+, respectively.

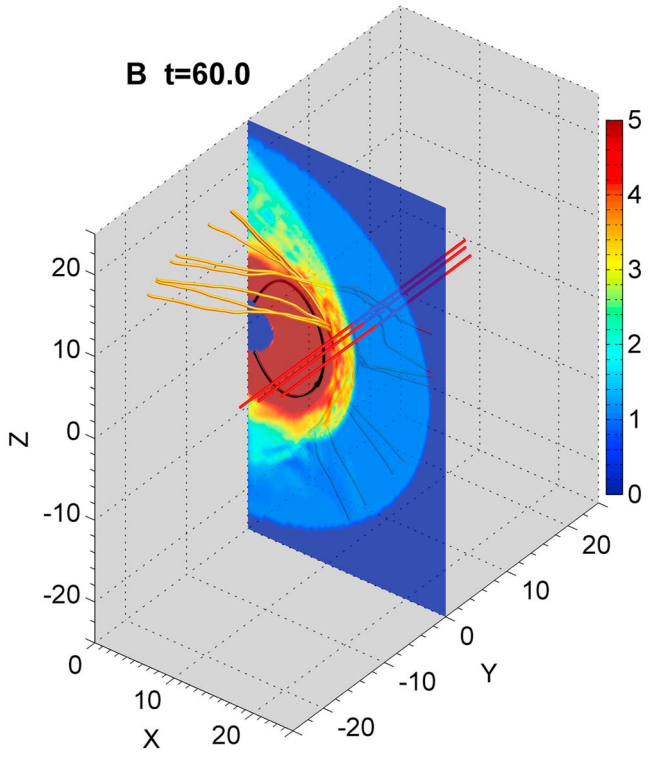

Figure 12. Contours of B in the noon meridian plane obtained at t = 60.0 obtained from case 5 with $\Delta\Phi = 90^{\circ}$, together with magnetic field lines, with the black lines being the magnetic field lines around the magnetopause, the orange lines the field lines of the transmitted tangential discontinuity in the magnetosheath, and red lines the field lines in the solar wind.

from the magnetopause downstream of the Q-|| (Q-⊥) shock in the case with $\Delta\Phi = 180^{\circ}$ and $w = 10d_{i0}$, and the length of the flux ropes is about $10R_E$ ($27R_E$) downstream of the Q-|| (Q-⊥) shock.

(3). For a fixed $\Delta\Phi = 180^{\circ}$, magnetosheath flux ropes are found downstream of both Q-|| and Q-⊥ shocks in the case with $w = 10d_{i0}$ in the solar wind. Nevertheless, under a relatively thick initial TD with $w = 30d_{i0}$, the convective compression is not enough to drive the magnetosheath reconnection, and the magnetic flux ropes cannot be found downstream of the Q-|| shock.

(4). For a fixed $w = 10d_{i0}$, when the field rotation angle decreases to $\Delta\Phi = 120^{\circ}$, magnetosheath flux ropes cannot be found downstream of the Q-|| shock, although there still exist flux ropes downstream of the Q-⊥ shock.

(5). When the rotation angle decreases to $\Delta\Phi = 90^{\circ}$, magnetic reconnection ceases to be seen in the entire magnetosheath.

(6). Our results indicate a longer length of magnetic flux ropes under a larger rotation angle $\Delta\Phi$. There exists a dawn-dusk asymmetry in the spatial extent of the magnetosheath flux ropes. Such asymmetry becomes more significant as the rotation angle $\Delta\Phi$ of magnetic field through the TD decreases.

(7). As the southward magnetic fluxes of the transmitted TD (on the sunward side) reaches and interacts with the magnetopause, magnetopause reconnection is initiated, forming magnetic flux ropes. These magnetopause flux ropes can wrap and mix with the magnetosheath flux ropes. The scale lengths of the magnetosheath ropes are significantly larger than the sizes of magnetopause in the dawn-dusk direction, but nearly comparable with those of the magnetopause flux ropes in both the radial and latitudinal directions.

DD, primarily RD or directional TD, is a commonly observed phenomenon in the interplanetary space. Our simulation has shown that magnetosheath reconnection may takes place when a transmitted TD passes through the bow shock toward magnetopause. As a consequence, the interaction between the interplanetary discontinuity and the magnetosphere is more complicated than a simple IMF change at the magnetopause. This result provides a mechanism of multiple processes for TD to interact with the bow shock/magnetopause.

Our simulation has demonstrated that the effects of a southward turning of the IMF may not be a simple magnetic field direction change at the magnetopause, and so not a simple occurrence of the reconnection process at the magnetopause. Rather, magnetic reconnection may be initiated in the global magnetosheath prior to the magnetopause reconnection due to the interaction of the bow shock and magnetosheath with the interplanetary TD. Near the magnetopause, the magnetosheath flux ropes can be mixed with the magnetopause flux ropes, and the scale lengths of them are approximately equal in both the radial and latitudinal directions.

It is also indicated in our simulation that there exists a critical field rotation angle of the incident TD, $\Delta\Phi = 90^{\circ}$, so that no reconnection flux ropes can be found in the magnetosheath if the rotation angle is below this value. Previously, Lin (1997) carried out a 2-D global hybrid simulation to study the interaction of the BS (Bow Shock) with a directional interplanetary discontinuity, and found little reconnection when the field rotation angle $\Delta\Phi$ is smaller than 80°. The difference between our result and that of Lin (1997) may be mainly due to the different orientations of the original IMF and the different dimensions of the two simulation models. In the simulation of Lin (1997), the initial IMF is in the xy plane, with $B_{x0} = B_{y0} = -0.707B_0$ and $B_{z0} = 0$. In our simulation, the initial IMF is in the xz plane with $B_{x0} = -0.5B_0$ and $B_{z0} = 0.866B_0$, which makes an angle of 30° with the $+z$ direction, and $B_{y0} = 0$. Moreover, our investigation is carried out for the 3-D physics.

The TD is compressed by the Q-⊥ shock and then undergoes a subsequent convective compression during its motion to the magnetopause. The formation of reconnection flux ropes in the transmitted TD downstream of

the Q-⊥ shock is consistent with the earlier observation and simulation results (Omidi et al., 2009; Pang et al., 2010; Phan et al., 2007). Our simulation indicates that the reconnected flux ropes are also present downstream of the Q-|| shock, at a distance much closer to the magnetopause than those at the Q-⊥ shock. For flux ropes downstream of the Q-|| shock, more time is necessary to compress the transmitted TD to thin enough in order to trigger magnetic reconnection because for these structures the convective compression is the dominant compression mechanism. The reconnection flow and magnetosheath flow determine the movement of the magnetosheath flux ropes, roughly along the plane of the current sheet.

On the dawn side of the magnetosheath, plasma flows are mainly pointed dawnward and tailward. Duskward and tailward plasma flows appear on the dusk side of the magnetosheath. Consider the sheet of a transmitted TD sheet along the y direction in general. With the presence of the Hall electric field E_x, the magnetic flux and ions gain a dawnward (in the $-y$ direction) $E \times B$ drift velocity, associated with E_x and B_z, both earthward and sunward of the transmitted TD current sheet center in the magnetosheath (similar to that in the magnetotail discussed by Lin et al., 2014). The direction of the magnetosheath flows are the same as that of the electric field drift velocity on the dawn side of the magnetosheath, and opposite to the electric field drift velocity on the dusk side. As a result, the accumulation of the magnetic flux and plasma is easier on the dusk-side ($+y$), which makes it harder to compress the transmitted TD and trigger magnetic reconnection. For this reason, the spatial extent of the flux ropes exhibits a dawn-dusk asymmetry in the magnetosheath.

Acknowledgments
This work was supported by the National Basic Research Program of China (2014CB845903), the National Science Foundation of China (Grant 41674168, 41804160, 41590851), and the grants NASA-80NSSC17K0012 and NASA-NNX17AI47G and DoE grant DE-FOA-0001664 to Auburn University, China Postdoctoral Science Foundation Funded Project (2018M630198). We thank Mingyu Wu for discussions and suggestions on our paper. The computer resources were provided by the National Supercomputer Center of China. The results in this paper are generated from our computer simulation code as described in section 2. The numerical data used for generating the presented figures are available via https://pan.baidu.com/s/1i8g1omaUlHANjjN_igKXeQ.

References

Angelopoulos, V., McFadden, J. P., Larson, D., Carlson, C. W., Mende, S. B., Frey, H., Phan, T., et al. (2008). Tail reconnection triggering substorm onset. *Science*, *321*, 931–935. https://doi.org/10.1126/science.1160495

Ashour-Abdalla, M., El-Alaoui, M., Goldstein, M. L., Zhou, M., Schriver, D., Richard, R., Walker, R., et al. (2011). Observations and simulations of non-local acceleration of electrons in magnetotail magnetic reconnection events. *Nature Physics*, *7*, 360–365. https://doi.org/10.1038/nphys1903

Behannon, K. W., Neubauer, F. M., & Barnstorf, H. (1981). Fine-scale characteristics of interplanetary sector boundaries. *Journal of Geophysical Research*, *86*, 3273–3287. https://doi.org/10.1029/JA086iA05p03273

Birn, J., Drake, J. F., Shay, M. A., Rogers, B. N., Denton, R. E., Hesse, M., Kuznetsova, M., et al. (2001). Geospace environment modeling (GEM) magnetic reconnection challenge. *Journal of Geophysical Research*, *106*, 3715–3719. https://doi.org/10.1029/1999JA900449

Biskamp, D. (2000). *Magnetic reconnection in plasmas*. Cambridge, UK: Cambridge University Press. https://doi.org/10.1017/CBO9780511599958

Burch, J. L., Torbert, R. B., Phan, T. D., Chen, L. J., Moore, T. E., Ergun, R. E., Eastwood, J. P., et al. (2016). Electron-scale measurements of magnetic reconnection in space. *Science*, *352*(6290), aaf2939. https://doi.org/10.1126/science.aaf2939

Burlaga, L. F. (1969). Directional discontinuities in the interplanetary magnetic field. *Solar Physics*, *7*, 54–71. https://doi.org/10.1007/BF00148406

Burlaga, L. F. (1971). On the nature and origin of directional discontinuities. *Journal of Geophysical Research*, *76*, 4360–4365. https://doi.org/10.1029/JA076i019p04360

Burlaga, L. F., Lemaire, J. F., & Turner, J. M. (1977). Interplanetary current sheets at 1 AU. *Journal of Geophysical Research*, *82*, 3191–3200. https://doi.org/10.1029/JA082i022p03191

Davis, M. S., Phan, T. D., Gosling, J. T., & Skoug, R. M. (2006). Detection of oppositely directed reconnection jets in a solar wind current sheet. *Geophysical Research Letters*, *33*, L19102. https://doi.org/10.1029/2006GL026735

Dungey, J. W. (1961). Interplanetary magnetic field and the auroral zones. *Physical Review Letters*, *6*, 47–48. https://doi.org/10.1103/PhysRevLett.6.47

Eastwood, J. P., Sibeck, D. G., Angelopoulos, V., Phan, T. D., Bale, S. D., McFadden, J. P., Cully, C. M., et al. (2008). THEMIS observations of a hot flow anomaly: Solar wind, magnetosheath, and ground-based measurements. *Geophysical Research Letters*, *35*, L17S03. https://doi.org/10.1029/2008GL033475

Eastwood, J. P., Sibeck, D. G., Slavin, J. A., Goldstein, M. L., Lavraud, B., Sitnov, M., Imber, S., et al. (2005). Observations of multiple X-line structure in the Earth's magnetotail current sheet: A cluster case study. *Geophysical Research Letters*, *32*, L11105. https://doi.org/10.1029/2005GL022509

Facskó, G., Kecskeméty, K., Erdős, G., Tátrallyay, M., Daly, P. W., & Dandouras, I. (2008). A statistical study of hot flow anomalies using Cluster data. *Advances in Space Research*, *41*(8), 1286–1291. https://doi.org/10.1016/j.asr.2008.02.005

Fu, X., Lu, Q., & Wang, S. (2006). The process of electron acceleration during collisionless magnetic reconnection. *Physics of Plasmas*, *13*, 012309. https://doi.org/10.1063/1.2164808

Gosling, J. T., Eriksson, S., Blush, L. M., Phan, T. D., Luhmann, J. G., McComas, D. J., Skoug, R. M., et al. (2007). Five spacecraft observations of oppositely directed exhaust jets from a magnetic reconnection X-line extending 4.26×10^6 km in the solar wind at 1 AU. *Geophysical Research Letters*, *34*, L20108. https://doi.org/10.1029/2007GL031492

Gosling, J. T., Eriksson, S., McComas, D. J., Phan, T. D., & Skoug, R. M. (2007). Multiple magnetic reconnection sites associated with a coronal mass ejection in the solar wind. *Journal of Geophysical Research*, *112*, 10111. https://doi.org/10.1029/2007JA012418

Gosling, J. T., Skoug, R. M., McComas, D. J., & Smith, C. W. (2005). Direct evidence for magnetic reconnection in the solar wind near 1 AU. *Journal of Geophysical Research*, *110*, A01107. https://doi.org/10.1029/2004JA010809

Greene, J. M. (1992). Locating three-dimensional roots by a bisect ion method. *Journal of Computational Physics*, *98*, 194–198. https://doi.org/10.1016/0021-9991(92)90137-N

Hasegawa, H., Wang, J., Dunlop, M. W., Pu, Z. Y., Zhang, Q. H., Lavraud, B., Taylor, M. G. G. T., et al. (2010). Evidence for a flux transfer event generated by multiple X-line reconnection at the magnetopause. *Geophysical Research Letters*, *37*, L16101. https://doi.org/10.1029/2010GL044219

Hasegawa, H., Zhang, H., Lin, Y., Sonnerup, B. U. Ö., Schwartz, S. J., Lavraud, B., & Zong, Q. G. (2012). Magnetic flux rope formation within a magnetosheath hot flow anomaly. *Journal of Geophysical Research*, *117*, A09214. https://doi.org/10.1029/2012JA017920

Huang, C., Wu, M., & Lu, Q. (2015). Electron acceleration in the dipolarization front driven by magnetic reconnection. *Journal of Geophysical Research: Space Physics*, *120*, 1759–1765.

Lee, L. C., Ma, Z. W., Fu, Z. F., & Otto, A. (1993). Topology of magnetic flux ropes and formation of fossil flux-transfer events and boundary layer plasma. *Journal of Geophysical Research*, *98*(A3), 3943–3951. https://doi.org/10.1029/92JA02203

Lepping, R. P., & Behannon, K. W. (1986). Magnetic field directional discontinuities: Characteristics between 0.46 and 1.0 AU. *Journal of Geophysical Research*, *91*, 8725–8741. https://doi.org/10.1029/JA091iA08p08725

Lin, Y. (1997). Generation of anomalous flows near the bow shock by its interaction with interplanetary discontinuities. *Journal of Geophysical Research*, *102*, 24,265–24,281. https://doi.org/10.1029/97JA01989

Lin, Y. (2002). Global hybrid simulation of hot flow anomalies near the bow shock and in the magnetosheath. *Planetary and Space Science*, *50*, 577–591. https://doi.org/10.1016/S0032-0633(02)00037-5

Lin, Y., & Wang, X. Y. (2005). Three-dimensional global hybrid simulation of dayside dynamics associated with the quasi-parallel bow shock. *Journal of Geophysical Research*, *110*, A12216. https://doi.org/10.1029/2005JA011243

Lin, Y., Wang, X. Y., Lu, S., Perez, J. D., & Lu, Q. (2014). Investigation of storm time magnetotail and ion injection using three-dimensional global hybrid simulation. *Journal of Geophysical Research: Space Physics*, *119*, 7413–7432. https://doi.org/10.1002/2014JA020005

Lin, Y. L., Lee, C., & Yan, M. (1996). Generation of dynamic pressure pluses downstream of the bow shock by variations in the interplanetary magnetic field orientation. *Journal of Geophysical Research*, *101*, 479–493. https://doi.org/10.1029/95JA02985

Lu, S., Angelopoulos, V., & Fu, H. (2016). Superthermal particle energization in dipolarization fronts: Particle-in-cell simulations. *Journal of Geophysical Research: Space Physics*, *121*, 9483–9500. https://doi.org/10.1002/2016JA022815

Lyons, L. R., Blanchard, G. T., Samson, J. C., Lepping, R. P., Yamamoto, T., & Moretto, T. (1997). Coordinated observations demonstrating external substorm triggering. *Journal of Geophysical Research*, *102*, 27,039–27,051. https://doi.org/10.1029/97JA02639

Maynard, N. C., Burke, W., Sandholt, P., Moen, J., Ober, D. M., Lester, M., Weimer, D. R., et al. (2001). Observations of simultaneous effects of merging in both hemispheres. *Journal of Geophysical Research*, *106*, 24,551–24,577. https://doi.org/10.1029/2000JA000315

Maynard, N. C., Sonnerup, B. U. Ö., Siscoe, G. L., Weimer, D. R., Siebert, K. D., Erickson, G. M., White, W. W., et al. (2002). Predictions of magnetosheath merging between IMF field lines of opposite polarity. *Journal of Geophysical Research*, *107*(A12), 1456. https://doi.org/10.1029/2002JA009289

Mozer, F. S., Bale, S. D., & Phan, T. D. (2002). Evidence of diffusion regions at a subsolar magnetopause crossing. *Physical Review Letters*, *89*(1), 015002. https://doi.org/10.1103/PhysRevLett.89.015002

Nagai, T., Fujimoto, M., Saito, Y., Machida, S., Terasawa, T., Nakamura, R., Yamamoto, T., et al. (1998). Structure and dynamics of magnetic reconnection for substorm onsets with geotail observations. *Journal of Geophysical Research*, *103*, 4419–4440. https://doi.org/10.1029/97JA02190

Nagai, T., Shinohara, I., Fujimoto, M., Hoshino, M., Saito, Y., Machida, S., & Mukai, T. (2001). Geotail observations of the hall current system: Evidence of magnetic reconnection in the magnetotail. *Journal of Geophysical Research*, *106*, 25,929–25,949. https://doi.org/10.1029/2001JA900038

Nakamura, R., Baumjohann, W., Asano, Y., Runov, A., Balogh, A., Owen, C. J., Fazakerley, A. N., et al. (2006). Dynamics of thin current sheets associated with magnetotail reconnection. *Journal of Geophysical Research*, *111*, A11206. https://doi.org/10.1029/2006JA011706

Øieroset, M., Phan, T. D., Fujimoto, M., Lin, R. P., & Lepping, R. P. (2001). In situ detection of collisionless reconnection in the Earth's magnetotail. *Nature*, *412*, 414–417. https://doi.org/10.1038/35086520

Omidi, N., Phan, T., & Sibeck, D. G. (2009). Hybrid simulations of magnetic reconnection initiated in the magnetosheath. *Journal of Geophysical Research*, *114*, A02222. https://doi.org/10.1029/2008JA013647

Omidi, N., Zhang, H., Chu, C., Sibeck, D., & Turner, D. (2014). Parametric dependencies of spontaneous hot flow anomalies. *Journal of Geophysical Research: Space Physics*, *119*, 9823–9833. https://doi.org/10.1002/2014JA020382

Omidi, N., Zhang, H., Sibeck, D., & Turner, D. (2013). Spontaneous hot flow anomalies at quasi-parallel shocks: 2. Hybrid simulations. *Journal of Geophysical Research: Space Physics*, *118*, 173–180. https://doi.org/10.1029/2012JA018099

Osman, K. T., Matthaeus, W. H., Gosling, J. T., Greco, A., Servidio, S., Hnat, B., Chapman, S. C., et al. (2014). Magnetic reconnection and intermittent turbulence in the solar wind. *Physical Review Letters*, *112*(21), 215002. https://doi.org/10.1103/PhysRevLett.112.215002

Pang, Y., Lin, Y., Deng, X. H., Wang, X. Y., & Tan, B. (2010). Three-dimensional hybrid simulation of magnetosheath reconnection under northward and southward interplanetary magnetic field. *Journal of Geophysical Research*, *115*, A03203. https://doi.org/10.1029/2009JA014415

Paschmann, G., Haerendel, G., Sckopke, N., Möbius, E., Lühr, H., & Carlson, C. W. (1988). Three-dimensional plasma structures with anomalous flow directions near the Earth's bow shock. *Journal of Geophysical Research*, *93*, 11279. https://doi.org/10.1029/JA093iA10p11279

Paschmann, G., Papamastorakis, I., Sckopke, N., Haerendel, G., Bame, S. J., Asbridge, J. R., Gosling, J. T., et al. (1979). Plasma acceleration at the Earth's magnetopause—Evidence for reconnection. *Nature*, *282*, 243–246. https://doi.org/10.1038/282243a0

Phan, T., Dunlop, M., Paschmann, G., Klecker, B., Bosqued, J. M., Rème, H., Balogh, A., et al. (2004). Cluster observations of continuous reconnection at the magnetopause under steady interplanetary magnetic field conditions. *Annales de Geophysique*, *22*, 2355–2367. https://doi.org/10.5194/angeo-22-2355-2004

Phan, T. D., Gosling, J. T., Davis, M. S., Skoug, R. M., Øieroset, M., Lin, R. P., Lepping, R. P., et al. (2006). A magnetic reconnection X-line extending more than 390 Earth radii in the solar wind. *Nature*, *439*, 175–178. https://doi.org/10.1038/nature04393

Phan, T. D., Kistler, L. M., Klecker, B., Haerendel, G., Paschmann, G., Sonnerup, B. U. Ö., Baumjohann, W., et al. (2000). Extended magnetic reconnection at the Earth's magnetopause from detection of bi-directional jets. *Nature*, *404*, 848–850. https://doi.org/10.1038/35009050

Phan, T. D., Love, T. E., Gosling, J. T., Paschmann, G., Eastwood, J. P., Oieroset, M., Angelopoulos, V., et al. (2011). Triggering of magnetic reconnection in a magnetosheath current sheet due to compression against the magnetopause. *Geophysical Research Letters*, *38*, L17101. https://doi.org/10.1029/2011GL048586

Phan, T. D., Paschmann, G., Twitty, C., Mozer, F. S., Gosling, J. T., Eastwood, J. P., Øieroset, M., et al. (2007). Evidence for magnetic reconnection initiated in the magnetosheath. *Geophysical Research Letters*, *34*, L14104. https://doi.org/10.1029/2007GL030343

Retinò, A., Nakamura, R., Vaivads, A., Khotyaintsev, Y., Hayakawa, T., Tanaka, K., Kasahara, S., et al. (2008). Cluster observations of energetic electrons and electromagnetic fields within a reconnecting thin current sheet in the Earth's magnetotail. *Journal of Geophysical Research*, *113*, A12215. https://doi.org/10.1029/2008JA013511

Retinò, A., Sundkvist, D., Vaivads, A., Mozer, F., André, M., & Owen, C. J. (2007). In situ evidence of magnetic reconnection in turbulent plasma. *Nature Physics*, *3*, 235–238. https://doi.org/10.1038/nphys574

Retinò, A., Vaivads, A., & Bale, S. D. (2007). Dissipation in turbulent plasma due to reconnection in thin current sheets. *Physical Review Letters*, *99*, 025004. https://doi.org/10.1103/PhysRevLett.99.025004

Russell, C. T., & Elphic, R. C. (1979). ISEE observations of flux transfer events at the dayside magnetopause. *Geophysical Research Letters*, *6*, 33–36. https://doi.org/10.1029/GL006i001p00033

Schwartz, S. J. (1995). Hot flow anomalies near the Earth's bow shock. *Advances in Space Research*, *158/9*, 107.

Schwartz, S. J., Kessel, R. L., Brown, C. C., Woolliscrofr, L. J. C., Dunplo, M. W., Farrugia, C. J., & Hall, D. S. (1988). Active current sheets near the Earth's bow shock. *Journal of Geophysical Research*, *93*(11), 295.

Sibeck, D. G., Phan, T.-D., Lin, R., Lepping, R. P., & Szabo, A. (2002). Wind observations of foreshock cavities: A case study. *Journal of Geophysical Research*, *107*(A10), 107, 1271. https://doi.org/10.1029/2001JA007539

Swift, D. W. (1996). Use of a hybrid code for global-scale plasma simulation. *Journal of Computational Physics*, *126*(1), 109–121. https://doi.org/10.1006/jcph.1996.0124

Thomsen, M. F., Borovsky, J. E., & Skoug, R. M. (2003). Delivery of cold, dense plasma sheet material into the near-Earth region. *Journal of Geophysical Research*, *108*(A4), 1151. https://doi.org/10.1029/2002JA009544

Thomsen, M. F., Gosling, J. T., Bame, S. J., Quest, K. B., Russell, C. T., & Fuselier, C. T. (1988). On the origin of hot diamagnetic cavities near Earth's bow shock. *Journal of Geophysical Research*, *93*(11), 311.

Thomsen, M. F., Gosling, J. T., Fuselier, S. A., Bame, S. J., & Russell, C. T. (1986). On the origin of hot diamagnetic cavities near Earth's bow shock. *Journal of Geophysical Research*, *91*, 1962.

Tsurutani, B. T., & Smith, E. F. (1979). Interplanetary discontinuities: Temporal variations and the radial gradient from 1 to 8.5 AU. *Journal of Geophysical Research*, *84*, 2773–2787. https://doi.org/10.1029/JA084iA06p02773

Wang, R., Lu, Q., Nakamura, R., Huang, C., du, A., Guo, F., Teh, W., et al. (2016). Coalescence of magnetic flux ropes in the ion diffusion region of magnetic reconnection. *Nature Physics*, *12*(3), 263. https://doi.org/10.1038/nphys3578

Wang, R., Nakamura, R., Lu, Q., Baumjohann, W., Ergun, R. E., Burch, J. L., Volwerk, M., et al. (2017). Simultaneously observed ion- and electron-scale quadrants of the reconnection hall magnetic field at magnetopause. *Physical Review Letters*, *118*, 175101. https://doi.org/10.1103/PhysRevLett.118.175101

Wu, M., Lu, Q., Volwerk, M., VöRöS, Z. N., Zhang, T., Shan, L., & Huang, C. (2013). A statistical study of electron acceleration behind the dipolarization fronts in the magnetotail. *Journal of Geophysical Research: Space Physics*, *118*, 4804–4810. https://doi.org/10.1002/jgra.50456

Xiao, C. J., Wang, X. G., Pu, Z. Y., Zhao, H., Wang, J. X., Ma, Z. W., Fu, S. Y., et al. (2006). In situ evidence for the structure of the magnetic null in a 3D reconnection event in the Earth's magnetotail. *Nature Physics*, *2*, 478–483. https://doi.org/10.1038/nphys342

Yordanova, E., Vörös, Z., Varsani, A., Graham, D. B., Norgren, C., Khotyaintsev, Y. V., Vaivads, A., et al. (2016). Electron scale structures and magnetic reconnection signatures in the turbulent magnetosheath. *Geophysical Research Letters*, *43*, 5969–5978. https://doi.org/10.1002/2016GL069191